



# Changes in glacier dynamics in the northern Antarctic Peninsula since 1985

Thorsten Seehaus<sup>1</sup>, Alison J. Cook<sup>2</sup>, Aline B. Silva<sup>3</sup>, and Matthias Braun<sup>1</sup>

<sup>1</sup>Institute of Geography, Friedrich-Alexander-University Erlangen-Nuremberg, Wetterkreuz 15, 91058 Erlangen, Germany

<sup>2</sup>Department of Geography, Durham University, South Road, Durham DH1 3LE, UK

<sup>3</sup>Laboratório de Monitoramento da Criosfera, Universidade Federal do Rio Grande, Av. Itália, km 8, 96203-900, Rio Grande, Brazil

**Correspondence:** Thorsten Seehaus (thorsten.seehaus@fau.de)

Received: 28 March 2017 – Discussion started: 7 April 2017

Revised: 29 December 2017 – Accepted: 13 January 2018 – Published: 20 February 2018

**Abstract.** The climatic conditions along the northern Antarctic Peninsula have shown significant changes within the last 50 years. Here we present a comprehensive analysis of temporally and spatially detailed observations of the changes in ice dynamics along both the east and west coastlines of the northern Antarctic Peninsula. Temporal evolutions of glacier area (1985–2015) and ice surface velocity (1992–2014) are derived from a broad multi-mission remote sensing database for 74 glacier basins on the northern Antarctic Peninsula ( $< 65^\circ$  S along the west coast and north of the Seal Nunataks on the east coast). A recession of the glaciers by  $238.81 \text{ km}^2$  is found for the period 1985–2015, of which the glaciers affected by ice shelf disintegration showed the largest retreat by  $208.59 \text{ km}^2$ . Glaciers on the east coast north of the former Prince Gustav Ice Shelf extent in 1986 receded by only  $21.07 \text{ km}^2$  (1985–2015) and decelerated by about 58 % on average (1992–2014). A dramatic acceleration after ice shelf disintegration with a subsequent deceleration is observed at most former ice shelf tributaries on the east coast, combined with a significant frontal retreat. In 2014, the flow speed of the former ice shelf tributaries was 26 % higher than before 1996. Along the west coast the average flow speeds of the glaciers increased by 41 %. However, the glaciers on the western Antarctic Peninsula revealed a strong spatial variability of the changes in ice dynamics. By applying a hierarchical cluster analysis, we show that this is associated with the geometric parameters of the individual glacier basins (hypsometric indexes, maximum surface elevation of the basin, flux gate to catchment size ratio). The heterogeneous spatial pattern of ice dynamic evolutions at the north-

ern Antarctic Peninsula shows that temporally and spatially detailed observations as well as further monitoring are necessary to fully understand glacier change in regions with such strong topographic and climatic variances.

## 1 Introduction

During the last century, the northern Antarctic Peninsula (AP) and its outlying islands have undergone significant warming (Turner et al., 2005), leading to substantial glaciological changes. Skvarca et al. (1998) reported a significant increase in surface air temperatures at the northeastern AP in the period 1960–1997 and correlated it with the recession of the Larsen and Prince Gustav ice shelves (Fig. 1) and the observed retreat of tidewater glaciers on James Ross Island in the period 1975–1995 (Skvarca et al., 1995). However, a recent cooling trend on the AP was revealed by Oliva et al. (2017) and Turner et al. (2016) since the late 1990s. Shepherd et al. (2012) compiled a comprehensive glacier mass balance database of the polar ice sheets. The authors estimated a mass loss on the whole AP ( $< 73^\circ$  S) of  $-36 \pm 10 \text{ Gt a}^{-1}$  for the period 2005–2010, which corresponds to 35 % of the total mass loss of Antarctica. A projection of sea level rise contribution by the AP ice sheet amounts to 7–16 mm sea level equivalent by 2100 and 10–25 mm by 2200 (Barrand et al., 2013a). However, along the western AP and on the higher-elevation areas an increase in snow accumulation in the late 20th century was derived from ice cores – e.g., at Palmer Land ( $73.59^\circ$  S,  $70.36^\circ$  W; Thomas et al.,

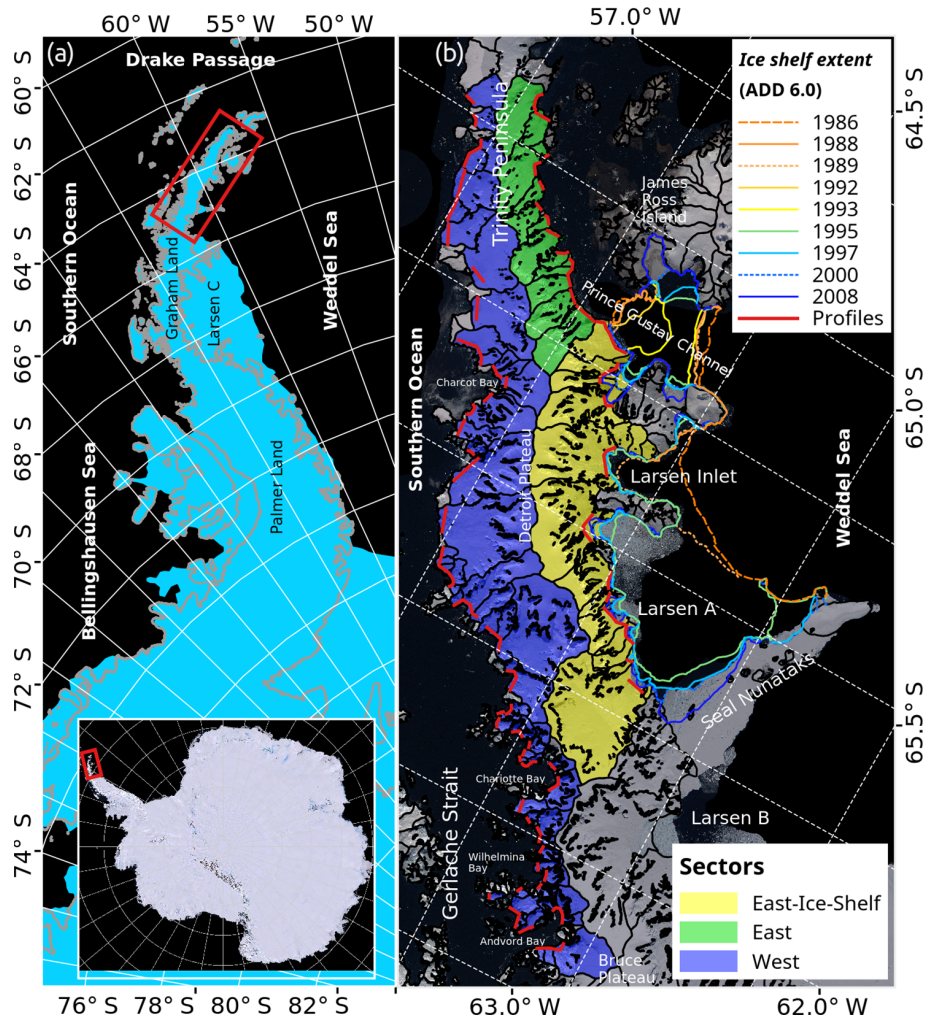


**Figure 1.** (a) Location of study site on the Antarctic Peninsula and on the Antarctic continent (inset). (b) Separation of study site in three sectors and retreat states of Prince Gustav and Larsen A ice shelves. Red lines: profiles at glacier front for velocity measurements. Map base, Landsat LIMA Mosaic USGS, NASA, BAS, NSF, coastlines (ice shelf extent) and catchment delineations are from SCAR Antarctic Digital Database 6.0.

2008), Detroit Plateau ( $64.08^{\circ}\text{S}$ ,  $59.68^{\circ}\text{W}$ ; Potocki et al., 2011) and at Bruce Plateau ( $66.03^{\circ}\text{S}$ ,  $64.07^{\circ}\text{W}$ ; Goodwind, 2013) – and climate models (e.g., Dee et al., 2011), whereas Van Wessem et al. (2016) obtained insignificant trends in precipitation.

Numerous ice shelves along the AP have retreated widely (e.g., Müller, Wilkins, Wordie) or disintegrated in recent decades (e.g., Larsen A in 1995, Larsen B in 2002) (Braun and Humbert, 2009; Cook and Vaughan, 2010; Doake and Vaughan, 1991; Rack et al., 1998; Rack and Rott, 2003; Wendt et al., 2010). As a consequence of the reduced buttressing, former tributary glaciers showed increased ice discharge and frontal retreat (e.g., De Angelis and Skvarca, 2003; Rack and Rott, 2004; Rignot et al., 2004; Seehaus et al., 2015; Wendt et al., 2010). For the northern AP ( $<66^{\circ}\text{S}$ ), a mass loss rate of  $-24.9 \pm 7.8 \text{ Gt a}^{-1}$  was reported by Scambos et al. (2014) for the period 2003–2008,

indicating that major ice mass depletion happened at the northern AP, especially along the eastern side, where numerous glaciers have been affected by ice shelf collapses. Seehaus et al. (2015, 2016) quantified the ice loss of former ice shelf tributaries. Mass loss rates of  $-2.14 \pm 0.21 \text{ Gt a}^{-1}$  (1995–2014) and  $-1.16 \pm 0.16 \text{ Gt a}^{-1}$  (1993–2014) were found at Dinsmoor–Bombardier–Edgeworth glacier system and Sjögren Inlet, respectively. Glaciers that were not terminating in an ice shelf also showed considerable changes. Cook et al. (2005, 2014) have analyzed the variations of tidewater glacier fronts since the 1940s. The authors reported that 90% of the observed glaciers retreated, which they partly attributed to atmospheric warming. A more recent study revealed a mid-ocean warming along the southwestern coast of the AP, forcing the glacier retreat in this region (Cook et al., 2016). Pritchard and Vaughan (2007) observed an acceleration of ice flow by  $\sim 12\%$  along the west coast

of the AP (1995–2005) and linked it to frontal retreat and dynamic thinning of the tidewater glaciers. Observations by Kunz et al. (2012) support this supposition. They analyzed surface elevation changes of 12 glaciers on the western AP based on stereoscopic digital elevation models (DEMs) over the period 1947–2010. Frontal surface lowering was found at all glaciers. Glacier-wide surface lowering was observed by various author groups (e.g., Berthier et al., 2012; Rott et al., 2014; Scambos et al., 2014) at former ice shelf tributaries along the northeastern AP. The collected observations suggest that the ice masses on the AP are contributing to sea level rise and show that glaciers' responses to climate change on the AP is not homogeneous and that more detailed knowledge of various aspects on the glacier changes is required. Previous studies often cover a specific period or area or focus on one particular aspect of glacier change. By now, the availability of remote sensing data, time series data and other datasets in this region facilitates the comprehensive analysis of glacier change. Therefore, we study the changes in glacier extent in combination with detailed investigations on ice dynamics as well as other derived geometrical attributes of glaciers on the northern AP ( $< 65^\circ$  S along the west coast and north of the Seal Nunataks on the east coast; Fig. 1b colored polygons) between 1985 and 2015. We analyze various multi-mission remote sensing datasets in order to obtain methodologically consistent and temporally detailed time series of ice dynamic changes of 74 glacier basins. The observations are individually discussed for the subregions, considering the different atmospheric, glaciological and oceanic conditions and changes.

## 2 Study site

The AP is the northern-most region of Antarctica and stretches from  $63$  to  $75^\circ$  S (Huber et al., 2017). It covers only 3 % of the entire continent in area but receives 13 % of the total mass input (Van Lipzig et al., 2002, 2004). The AP's mountain chain (typically 1500–2000 m high) acts as an orographic barrier for the circumpolar westerly air streams, leading to very high precipitation values on the west coast and on the plateau region of up to 5000 mm w.e.  $\text{a}^{-1}$ , as well as frequent foehn-type wind occurrences on the east coast (Cape et al., 2015; Marshall et al., 2006; Van Wessem et al., 2016). The foehn events are characterized by strong winds and high air temperatures. Consequently, the climatic mass balance ( $b_{\text{clim}}$ ) shows a strong gradient across the mountain chain (Turner, 2002; Van Wessem et al., 2016). Aside from those that are ice shelf tributaries, almost all glaciers on the AP are marine terminating, and the majority of the glacier catchments extend up to the high-elevation plateau regions (north to south: Laclavère, Louis Philippe, Detroit, Herbert, Foster, Forbidden, Bruce, Avery, Hemimont, Dyer). Typically the AP plateau is separated from the outlet glaciers by escarpments and ice falls. Glaciers on the west coast drain

**Table 1.** Abbreviations of glacier names.

Abbreviation	Glacier names
AMR	Arago–Moser–Rudolph
APPE	Albone–Pyke–Polaris–Eliason
CLM	Cayley–Lilienthal–Mouillard
DBE	Dinsmoor–Bombardier–Edgeworth
SBG	Sikorsky–Breguet–Gregory

into the Bellingshausen Sea and on the east coast into the Weddell Sea. Since the 1980s, the ice shelves along the east coast have substantially recessed and disintegrated (Larsen Inlet in 1987–1989, Prince Gustav and Larsen A in 1995 and Larsen B in 2002) (Cook and Vaughan, 2010; Rott et al., 1996; Skvarca et al., 1999), which Scambos et al. (2003) attributed to higher summer air temperatures and surface melt. A more recent study by Holland et al. (2015) discovered that significant thinning of the Larsen C Ice Shelf is caused by basal melting and that ungrounding from an ice rise and frontal recession could trigger its collapse. The northern AP has a maritime climate and is the only region of Antarctica that frequently experiences widespread surface melt (Bartrand et al., 2013b; Rau and Braun, 2002).

Our study site stretches approximately 330 km from the northern tip of the AP mainland southwards to Drygalski Glacier on the east coast and Grubb Glacier on the west coast (Fig. 1). This facilitates the analyses of the temporal evolution ( $\sim 20$  years) of the response of tributary glaciers to ice shelf disintegration at the former Larsen A and Prince Gustav ice shelves on the east coast, the investigation of glaciers north of the former Prince Gustav Ice Shelf, where no information on change in ice flow is currently available, and the comparison with temporal variations in ice dynamics along the west coast at the same latitude. The study site covers  $\sim 11\,000\text{ km}^2$  ( $\sim 11\%$  of the whole AP including islands; Cook et al., 2014; Huber et al., 2017) with elevations stretching from sea level up to 2220 m. The glacier basin delineations are based on the Antarctic Digital Database (ADD) 6.0 (Cook et al., 2014). Glacier names are taken from the Global Land Ice Measurements from Space (GLIMS) project database. The local GLIMS glacier IDs (e.g., TPE62, LAB2) are used for unnamed glaciers and further missing glacier basin names are replaced with the ADD 6.0 glacier IDs. Neighboring basins with coalescing ice flow at the termini are merged (many are already merged in ADD 6.0), as the delineation of the individual glacier sections is not always possible and the width can vary temporally (due to changes in mass flux of the individual glaciers). In these cases, the names of the glaciers are also merged (e.g., Sikorsky–Breguet–Gregory, SBG; see Table 1 for abbreviations of glacier names). Due to the sparse data coverage (fewer than three good-quality velocity measurements), no time series analysis of the glaciers at the northern tip of

**Table 2.** Overview of SAR sensors and specifications used in this study.

Platform	Sensor	Mode	SAR band	Repetition cycle (days)	Time interval	Ground range resolution (m) <sup>a</sup>	Tracking patch sizes ( $p \times p$ ) <sup>b</sup>	Tracking step size ( $p \times p$ ) <sup>b</sup>	Mean uncertainty of tracking results ( $\text{m d}^{-1}$ )
ERS-1/2	SAR	IM	C band	35/1	8 December 1992 2 April 2010	30	48 × 240 64 × 320	5 × 25	0.15 ± 0.10
RADARSAT 1	SAR	ST	C band	24	10 September 2000 3 September 2006	30	48 × 192 64 × 256	5 × 20	0.11 ± 0.03
Envisat	ASAR	IM	C band	35	5 December 2003 16 August 2009	30	32 × 160 64 × 320 128 × 640	5 × 25	0.12 ± 0.05
ALOS	PALSAR	FBS	L band	46	18 May 2006 17 March 2011	10	64 × 192 96 × 192 128 × 384	10 × 30	0.05 ± 0.06
TerraSAR-X TanDEM-X	SAR	SM	X band	11	14 October 2008 22 December 2014	3	128 × 128 256 × 256 512 × 512	25 × 25	0.06 ± 0.04

<sup>a</sup> Nominal resolution, dependent on the incidence angle.

<sup>b</sup> Intensity tracking parameters are provided in pixels ( $p$ ) in slant range geometry.

the AP or at some capes and peninsulas (e.g., Sobral Peninsula, Cape Longing) is possible. Therefore, the northernmost analyzed catchments are Broad Valley Glacier on the east coast and TPE8 Glacier on the west coast, resulting in 74 studied glacier basins. Furthermore, the study site is divided into three sectors, taking into account the different climatic settings and drainage orientation as well as former ice shelf extent: sector West, which contains glaciers on the west coast, draining into the Bransfield and Gerlache straits; sector East, which contains glaciers on the east coast, draining into the Prince Gustav Channel; and sector East-Ice-Shelf, which contains glaciers on the east coast that were former tributaries to the Larsen A, Larsen Inlet and Prince Gustav ice shelves.

### 3 Data and methods

A large number of various remote sensing datasets are analyzed in order to obtain temporally and spatially detailed information on changes in ice dynamics in the study area. Glacier area changes are derived from satellite and aerial imagery. Repeat-pass synthetic aperture radar (SAR) satellite acquisitions are used to compute surface velocity fields in order to obtain information on changes in glacier flow speed. Auxiliary data from sources such as a DEM and glacier inventory are included in the further analyses and discussion of the results.

#### 3.1 Area changes

Changes in glacier area are derived by differencing glacier outlines from various epochs. All observed glaciers are tide-water glaciers and only area changes along the calving front were considered. Information on the positions of the glacier fronts is taken from Cook et al. (2014) and is available for the

whole AP in ADD 6.0 (1945–2010). This coastal-change inventory is based on manually digitized ice-front positions using imagery from various satellites (e.g., Landsat, ERS) and aerial photo campaigns. This dataset is updated (up to 2015) and gaps are filled by manual mapping of the ice-front positions based on SAR and optical satellite images. Consistent with Cook et al. (2014), the ice-front positions are assigned to 5-year intervals in order to analyze temporal trends in glacier area changes in the period 1985–2015. Before 1985, only sparse information on ice-front positions for the whole study site is available, and the coverage by SAR data for analyzing glacier flow starts in 1992. Additionally, the analysis of the area changes for the Larsen A and Prince Gustav ice shelf tributaries is limited to the period 1995–2015, as the ice shelves disintegrated in 1995.

The uncertainties of the glacier change measurements strongly depend on the specifications of the imagery used (e.g., spatial resolution, geodetic accuracies) as well as the methods used. To each record in the coastal-change inventory from ADD 6.0, a reliability rating is assigned according to Ferrigno et al. (2006). The rating ranges from 1 to 5 (reliability within 60 m to 1 km) and takes into account errors due to manual digitization and interpretation (see Ferrigno et al., 2006, for a detailed description). This approach is also applied on the updated ice-front positions. Nearly all mapped ice fronts in the area studied have a good reliability rating of 1 (76 %) and 2 (21 %). Only a few glacier fronts (3 %) have a rating of 3. No ice fronts with reliability ratings of 4 and 5 are mapped in the study area.

#### 3.2 Surface velocities

Surface velocity maps are derived from repeat-pass SAR acquisitions. SAR image time series of the satellite missions ERS-1/2, Envisat,

RADARSAT-1, ALOS, TerraSAR-X (TSX) and TanDEM-X (TDX) are analyzed, covering the period 1992–2014. Specifications of the SAR sensors are listed in Table 2. The large number of SAR images were provided by the German Aerospace Center (DLR), the European Space Agency (ESA) and the Alaska Satellite Facility (ASF). To obtain displacement fields for the glaciers, the widely used and well-approved intensity offset tracking method is applied on co-registered single look complex SAR image pairs (Strozzi et al., 2002). In order to improve the co-registration of the image pairs, we mask out fast-moving and unstable regions such as outlet glaciers and the sea during the co-registration processes. Furthermore, single SAR image tiles acquired during the same satellite flyover are concatenated in the along-track direction. This helps to further improve the co-registration in coastal regions (by including more stable areas in the co-registration process) but also simplifies the analysis of the final results as no mosaicking of the results is needed. Image pairs with low-quality co-registration are filtered out. A moving window technique (step-size; see Table 2) is used by the intensity offset tracking method to compute the cross-correlation function of each image patch and to derive its azimuth and slant range displacement. The resolution of the obtained displacement fields depends on the combination of the step-size and the resolution of the images in slant range geometry. A resolution of the velocity fields of  $\sim 50$  m for the high-resolution sensors TSX, TDX and  $\sim 100$  m for all other sensors was targeted. Less reliable offset measurements are filtered out by means of the signal-to-noise ratio of the normalized cross-correlation function. Moreover, we apply an additional filter algorithm based on a comparison of the magnitude and alignment of the displacement vector relative to its surrounding offset measurements. This technique removes more than 90 % of incorrect measurements (Burgess et al., 2012). Finally, the displacement fields are transferred from slant range into ground range geometry, taking into account the contortion caused by the topography (topographic effects on the local SAR incidence angle). The results are then geocoded, orthorectified, resampled and converted into velocity fields (with 100 m pixel spacing for all sensors) by means of the time span between the SAR acquisitions. The mean date of the consecutive SAR acquisitions is assigned to each velocity field. The ASTER Global DEM of the Antarctic Peninsula (AP-DEM; Cook et al., 2012) is used as elevation reference. It is currently the best available DEM of the Antarctic Peninsula. It has a mean elevation bias of  $-4$  m ( $\pm 25$  m RMSE) from ICESat data and horizontal accuracy better than 2 pixels. Since the accuracy varies regionally, Huber et al. (2017) estimated the uncertainty to be  $\pm 50$  m for the AP-DEM, based on their experiences with other DEMs. Velocity data are analyzed close to the calving front (see further down), where the slope of the glaciers at the AP is typically quite low. Thus, the impact of the DEM accuracy

on the velocity fields is insignificant (see Seehaus et al., 2015, Supplement).

Depending on the displacement rate and resolution of the SAR sensor, the tracking window size needs to be adapted (de Lange et al., 2007). For the fast-flowing central glacier sections, larger window sizes are needed since large displacements cannot be tracked by using small correlation patches. Small tracking window sizes are suitable for the slow-moving lateral sections of the outlet glaciers. Wide parts of large tracking patches cover the stable area next to the glacier, which biases the tracking results towards lower velocities. Consequently, we compute surface velocity fields of the same image pairs for different correlation patch sizes in order to get the best spatial coverage. Table 2 shows the different tracking window sizes for each sensor. The results of each image pair are stacked by starting with the results of smallest tracking window size and filling the gaps with the results of the next biggest tracking window size.

The accuracy of the velocity measurements strongly depends on the co-registration quality and the intensity offset tracking algorithm settings. The mismatch of the co-registration  $\sigma_v^C$  is quantified by measuring the displacement on stable reference areas close to the coast line, such as rock outcrops and nunataks. Based on the Bedmap2 (Fretwell et al., 2013) and ADD 6.0 rock outcrop masks, reference areas are defined and the median displacements magnitude of each velocity field is measured at these areas. The uncertainty of the tracking process  $\sigma_v^T$  is estimated according to McNabb et al. (2012) and Seehaus et al. (2015) depending on accuracy of the tracking algorithm  $C$ , image resolution  $dx$ , oversampling factor  $z$  and time interval  $dt$ .

$$\sigma_v^T = \frac{C dx}{z dt}. \quad (1)$$

The accuracy of the tracking algorithm is estimated to be 0.2 pixels and an oversampling factor  $z = 2$  is applied to tracking patches in order to improve the accuracy of the tracking process. Both independent error estimates are quadratically summed to compute the uncertainties of the individual velocity fields  $\sigma_v$ .

$$\sigma_v = \sqrt{(\sigma_v^T)^2 + (\sigma_v^C)^2} \quad (2)$$

Two approaches to measure and analyze the temporal changes in ice flow of the studied glacier are evaluated (see also Sect. S1 in the Supplement).

In the first approach, an across glacier profile is defined (red lines in Fig. 1) close to the terminus of each basin, considering the maximum retreat state of the ice front in the observation period. The changes in the ice flow of the individual glaciers are analyzed by measuring the surface velocities along the profiles. In order to reduce the number of data gaps along the profile due to pixel size data voids in the velocity fields, the velocity data are extracted within a buffer

**Table 3.** Description of velocity change categories.

Category	Description	Rating*
Positive	General increase of flow speed	2
Peak	Increase of flow speed with subsequent deceleration	1
Stable	Variability of measurements $< 0.25 \text{ m d}^{-1}$	0
Fluctuating	Short-term speed-ups and deceleration, no clear trend	0
Trough	Decrease of flow speed with subsequent acceleration	-1
Negative	General decrease of flow speed	-2

\* Ratings used for cluster analysis Sect. 3.4.

**Table 4.** Hypsometric index (HI) and glacier basin category descriptions.

HI*	Hypsometric categories	Number of glaciers
$\text{HI} < -1.5$	Very top heavy	8
$-1.5 < \text{HI} < -1.2$	Top heavy	7
$-1.2 < \text{HI} < 1.2$	Equidimensional	18
$1.2 < \text{HI} < 1.5$	Bottom heavy	13
$\text{HI} > 1.5$	Very bottom heavy	28

\* According to Jiskoot et al. (2009).

zone of 200 m around the profiles. The results are visually inspected in order to remove unreliable measurements, based on the magnitude and direction of ice flow along the profiles. Datasets with partial profile coverage, large data gaps or large-scale tracking errors are rejected. The resulting profile coverage by velocity measurements is on average 97 % and data coverage of more than 93 % is obtained for 90 % of all extracted profiles. To minimize the impact of potential outliers (still remaining tracking errors), median velocities along the profiles are calculated and their temporal developments are plotted for each basin (Figs. S1–S74 in the Supplement).

In the second approach, the velocity values are picked at the location of maximum ice thickness at the across glacier profiles (taken from the first approach). Ice thickness is obtained from the ice thickness reconstruction of the AP by Huss and Farinotti (2014). By means of visual inspection of the velocity profiles obtained by the first approach, outliers in the measurements using the second approach are manually filtered out and the resulting evolution of the flow speeds of each glacier are plotted (Figs. S75–S148 in the Supplement).

The glaciers are manually classified in six categories according to the temporal evolution of the ice flow speeds (see Table 3), since automatic classification attempts did not achieve satisfying results. Only glaciers with three or more observations and an observation period of more than 10 years are considered in the categorization, resulting in 74 cate-

gorized glacier basins (colored polygons in Fig. 1b). The GAMMA Remote Sensing software is used for processing of the SAR data.

### 3.3 Catchment geometries and settings

Glacier velocities and area change measurements provide information on the ice dynamics of the individual glaciers. To facilitate a better and comprehensive interpretation of these observations, additional attributes regarding the different geometries and settings of the glaciers are derived. In addition to glacier attributes derived by Huber et al. (2017), we calculated the hypsometric index (HI) and the ratio of the flux gate cross section divided by the glacier catchment area.

Mass input strongly affects the dynamics of a glacier. The climatic mass balance at the northern AP shows a strong spatial variability, with very high accumulation rates along the west coast ( $3769 \text{ mm w.e. a}^{-1}$  on average in sector West, 1992–2014, RACMO2.3), significantly lower values on the east coast ( $1119 \text{ mm w.e. a}^{-1}$  on average in sector East, 1992–2014, RACMO2.3) and an increase towards higher altitudes along both coast lines (Turner, 2002; Van Wessem et al., 2016). Consequently, the mass input depends on the basin orientation (east coast or west coast), elevation range and the hypsometry. For each glacier basin an HI, defined by Jiskoot et al. (2009), is calculated by means of surface elevations from the AP-DEM. Based on this index the glaciers are grouped into the five categories according to Jiskoot et al. (2009), ranging from “very top heavy” to “very bottom heavy” (Table 4). Moreover, the maximum elevations of the individual glacier catchments are derived from the AP-DEM, which represents the altitude range of the catchment, since all observed glaciers are marine terminating.

In order to characterize the catchment shape, the ratios (FA) of the flux gate cross sections divided by the glacier catchment areas are calculated. The flux gates are defined along the profiles used for the glacier flow analysis (Sect. 3.2). Lower values of FA indicate a channelized outflow (narrowing towards the glacier front), whereas higher FA ratios imply a broadening of the glacier towards the calving front. Ice thickness at the flux gates is taken from the AP Bedmap dataset from Huss and Farinotti (2014).

### 3.4 Cluster analysis

The glaciers in sector West (Fig. 1, red shaded area) show a heterogeneous spatial pattern of ice dynamics as compared to the other sectors changes (Sects. 4.1 and 4.2). In order to analyze the influence of the glacier geometries on the glaciological changes and to find similarities, a cluster analysis is carried out in sector West. This is a proven method to classify glaciers based on a set of variables (Lai and Huang, 1989; Sagredo and Lowell, 2012). Variables of the glacier dynamics used are the derived area changes (in percent) and velocity changes (ratings of the categories, Table 3). Glaciers catego-

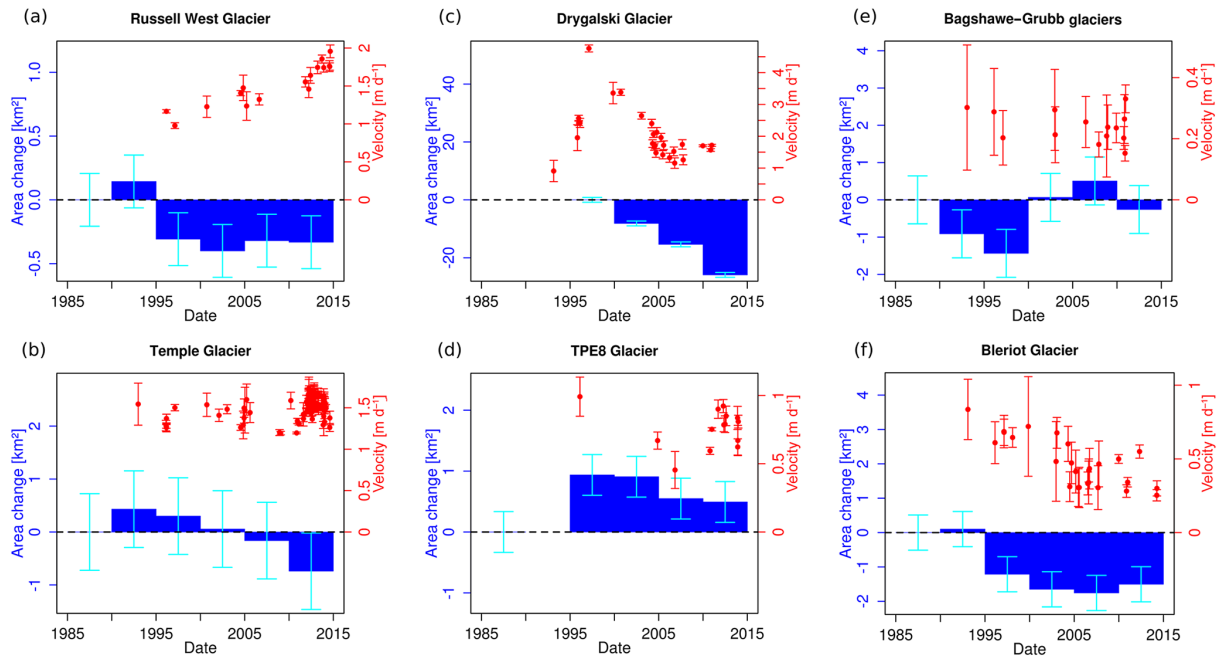


**Figure 2.** Temporal evolution of surface velocity (red, using first measuring approach) and area (blue) changes of selected glaciers in the study area for each velocity change category (see Table 3).

rized as “stable” showed a temporal variability in flow speeds of less than  $0.25 \text{ m d}^{-1}$ . Therefore, we used the same rating for the velocity change categories “stable” and “fluctuating” to perform the cluster analysis. The glacier geometry parameters used are the HI, maximum surface elevation  $h_{\text{max}}$  of the basin and the ratio of flux gate to catchment size, FA. The variables are standardized in the traditional way of calculating their standard scores (also known as  $z$  scores or normal scores). It is done by subtracting the variables mean value and dividing by its SD (Miligan and Cooper, 1988). Afterwards a dissimilarity matrix is calculated using the Euclidean distances between the observations (Deza and Deza, 2009). A hierarchical cluster analysis (Kaufman and Rousseeuw, 1990) is applied on the dissimilarities using Ward’s minimum variance method (Ward, 1963). At the start, the most similar glaciers (samples) are grouped. The resulting clusters are iteratively joined based on their similarities until only one cluster is left, resulting in a dendrogram (see Sect. 4.4). The distances between the clusters are updated in each iteration step by applying the Lance–Williams algorithms (Lance and Williams, 1967).

## 4 Results

### 4.1 Area changes

Area changes relative to the measurements in the epoch 1985–1989 (1995–2000 for the former Larsen A and Prince Gustav ice shelf tributaries; see Sect. 5.2) of the observed

**Table 5.** Summary of observed parameters for each sector and all glaciers.

Sector	East	East-Ice-Shelf	West	All glaciers
$N$	13	13	48	74
$l_f$ (m)	85 114	127 909	268 763	481 786
$A_{1985-1990}$ ( $\text{km}^2$ )	1538.78	3655.13	5809.33	11 003.23
$A_{2010-2015}$ ( $\text{km}^2$ )	1517.71	3446.54	5800.18	10 764.42
$dA$ ( $\text{km}^2$ )	−21.07	−208.59	−9.14	−238.81
$dt$ (a)	18.22	19.05	19.58	19.25
First velocity measuring approach				
$v_S$ ( $\text{m d}^{-1}$ )	0.729	0.480	0.428	0.490
$v_E$ ( $\text{m d}^{-1}$ )	0.306	0.562	0.605	0.545
$dv$ ( $\text{m d}^{-1}$ )	−0.423	0.081	0.177	0.055
$n_V$	277	550	1429	2256
Second velocity measuring approach				
$v_S$ ( $\text{m d}^{-1}$ )	1.834	0.760	0.831	0.994
$v_E$ ( $\text{m d}^{-1}$ )	0.562	1.071	1.200	1.065
$dv$ ( $\text{m d}^{-1}$ )	−1.272	0.312	0.369	0.071
$n_V$	355	639	1742	2736

$N$  – number of studied glaciers

$l_f$  – Length of ice front

$A$  – glacier area in the respective period (subscript)\*

$dA$  – change in glacier area between 1985 and 2015\*

$dt$  – mean time period of velocity measurements

$v_S$  – mean of earliest velocity measurements (1992–1996)

$v_E$  – mean of latest velocity measurements (2010–2014)

$dv$  – mean velocity change

$n_V$  – sum of velocity measurements in the observation period (dt)

\* Since 1995 for the former Larsen A and Prince Gustav ice shelf tributaries (see Sect. 5.2).

glaciers are plotted in Figs. S1–S74 in the Supplement. The glaciers are classified in three groups based on the latest area change measurements, which are illustrated in Fig. 2: re-

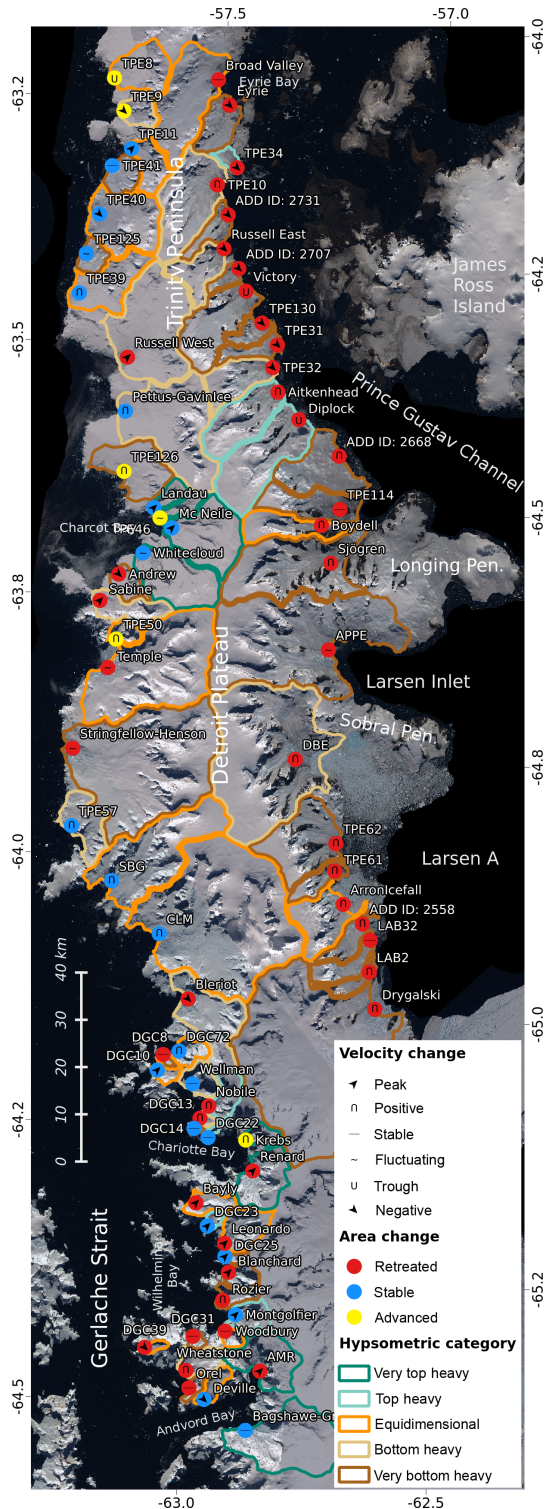


**Figure 3.** Categorizations of glaciers based on the temporal variations of area changes (dots) and flow velocities (symbols). Colors of catchment delineation indicate hypsometric categories according to Jiskoot et al. (2009). Background: Landsat LIMA Mosaic USGS, NASA, BAS, NSF.

treat (Fig. 2a–c and f), which is the loss of glacier area by frontal retreat; stable (Fig. 2e), in which there are no significant area changes (within the error bars); advance (Fig. 2d), in which there is a gain of glacier area by frontal advance. In Fig. 3 the spatial distribution of the area change classification is illustrated. All glaciers along the east coast, including the former ice shelf tributaries, retreated, whereas along the west coast numerous glaciers show stable ice-front positions and some glaciers even advanced. In total, 238.81 km<sup>2</sup> of glacier area was lost in the survey area in the period 1985–2015, which corresponds to a relative loss of 2.2%. All sectors show glacier area loss (Table 5), of which the area loss by 5.7% (208.59 km<sup>2</sup>) in sector East-Ice-Shelf clearly dominates. The glaciers in sectors West and East recessed by 0.2% (9.14 km<sup>2</sup>) and 1.4% (21.07 km<sup>2</sup>), respectively. The temporal trends of total glacier area and area loss of all observed glaciers and of each sector are presented in Fig. 4. Catchment areas and changes between 1985 and 2015 of the individual basins are listed in Table S1 in the Supplement and relative changes are illustrated in Fig. 5.

**4.2 Surface velocities**

A total of 282 stacked and filtered velocity fields are derived from the SAR acquisitions covering the period from 25 December 1992 until 16 December 2014. Figures S157–S160 in the Supplement show exemplary velocity fields of the studied area obtained for ERS, Envisat, ALOS and TSX–TDX data. The average total uncertainty of the velocity fields amounts to 0.08 ± 0.07 m d<sup>-1</sup> and the values for each SAR sensor are provided in Table 2. In Table S3 in the Supplement the error estimates of each velocity field are listed. The mean sample count to estimate the co-registration quality is 11 717 and the average mismatch amounts to 0.07 m d<sup>-1</sup>. The error caused by the tracking algorithm strongly varies depending on the source of the SAR data (sensor). A mean value of 0.05 m d<sup>-1</sup> is found. ERS image pairs with time intervals of 1 day have very large estimated tracking uncertainties, biased by the very short temporal baselines. Therefore, only the errors caused by the mismatch of the co-registration are considered in the total error computations of the seven ERS tracking results with 1-day temporal baselines.

All measured velocity profiles of the 74 observed glaciers are visually inspected and in total 2256 profile measurements (first approach) and 2736 point measurements (second approach) passed the quality check. The shortest observation period is 14.83 years at DBC31 Glacier, the average number of velocity measurements per glacier is 30.5 and 37.0 and the average observation period is 19.25 years (σ = 2.06 years) and 19.21 years (σ = 1.96 years) for the first and second measuring approach, respectively. Figure 2 shows by example the temporal evolution of the ice flow (using the first approach) for each velocity change category (see Table 3) and Figs. S149–S156 in the Supplement show surface velocity profiles across the terminus for the same glaciers as well

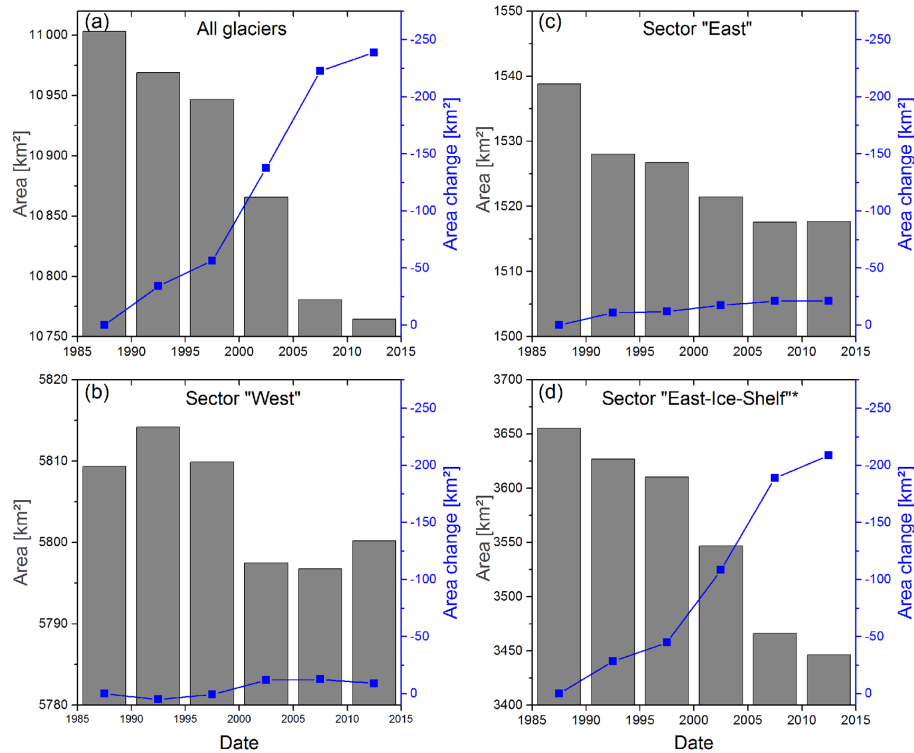


**Figure 4.** Total glacier area (gray bars) of the whole study site (a) and of the individual sectors (b–d) in the period 1985–2015. Changes in glacier area (blue points) are relative to the measurements in time interval 1985–1990. Note the different scaling of the left y axes. \* In sector East-Ice-Shelf, area changes before 1995 are only measured at Larsen Inlet tributaries (APPE glaciers).

as for the small glacier catchments DGC14 and TPE61. For small and narrow glaciers, the capturing of the flow velocity gradients in the margins is still limited mainly by the sensor resolution, even applying different tracking window sizes (see Sect. 3.2).

The temporal evolution of the surface velocities at the termini of each glacier are depicted in the Supplement (Figs. S1–S74 for the first approach, Figs. S75–148 for the second approach) and the related categories are listed in Tables S1 and S2 in the Supplement.

For both velocity measuring approaches and each glacier, the flow velocities in the first  $v_S$  and last year  $v_E$  of the observation period as well as the absolute and relative change  $dv$  is presented in Tables S1 and S2 in the Supplement. The mean values of  $v_S$ ,  $v_E$  and  $dv$  of all analyzed glaciers and for each sector are listed in Table 5. On average the ice flow in the whole studied area increased by  $0.061 \text{ m d}^{-1}$  (13 %) and  $0.071 \text{ m d}^{-1}$  (7 %) for the first and second approach, respectively, but the average changes of the individual sectors are more pronounced. Along the west coast an average acceleration by 41 % ( $0.177 \text{ m d}^{-1}$ ) and 44 % ( $0.369 \text{ m d}^{-1}$ ) occurred and the former ice shelf tributaries on the east coast accelerated by 26 % ( $0.118 \text{ m d}^{-1}$ ) and 41 % ( $0.312 \text{ m d}^{-1}$ ) for both approaches, respectively. In sector East the glaciers decelerated resulting in a mean velocity change of  $-58 \%$

( $-0.423 \text{ m d}^{-1}$ ) and  $-69 \%$  ( $-1.272 \text{ m d}^{-1}$ ) for the first and second approach, respectively. The presented average flow speed change values are based on the observed changes of all glaciers in the respective sector (Table S1 in the Supplement), ignoring the different size of the individual glaciers.

Detailed results and differences of both approaches to measure the glacier velocities are presented and discussed Sect. S1. Based on this discussion, we decided to favor the first approach and its results are used for the subsequent analysis.

The spatial distribution of the categories is illustrated in Fig. 3. At nearly all glaciers in sector East-Ice-Shelf a peak in ice velocities is observed. In sector East, most glaciers showed a decrease in flow velocities in the observation period. The glaciers on the west coast show a more irregular distribution than along the east coast, but a local clustering of accelerating glaciers can be observed at Wilhelmina Bay. In order to analyze the quality of obtained velocity change signal, the ratio of the maximum measured velocity difference (maximum velocity minus minimum velocity) divided by the average error of the velocity measurements is calculated for each glacier. An average signal-to-noise ratio of 14.6 is found. At three glaciers (DGC14, DGC22 and Orel) a signal-to-noise ratio of less than 2 is observed. These

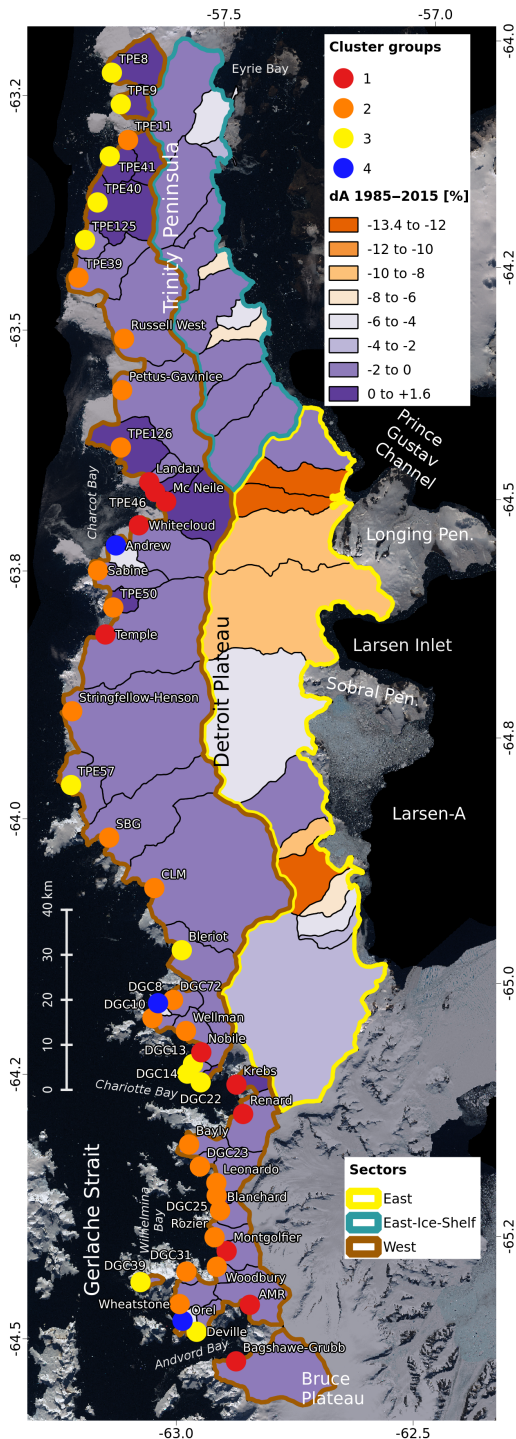


**Figure 5.** Spatial distribution of glacier types along the west coast. Glaciers are grouped based on a hierarchical cluster analysis (dots). In Sect. 5.3 the characteristics of the groups are discussed in detail. Individual glacier catchment colors indicate relative area change in the period 1985–2015. Colored polygon outlines indicate boundaries of the three sectors. Background: Landsat LIMA Mosaic USGS, NASA, BAS, NSF.

glaciers are characterized as stable, which justifies the low signal-to-noise ratio.

### 4.3 Catchment geometries and settings

The spatial distribution of HI and categories of the glacier basins is presented in Fig. 3 and the values are listed in Table S1 in the Supplement. The HI values range between  $-4.6$  and  $9.1$  (mean:  $0.88$ ,  $\sigma$ :  $2.10$ ). No clear spatial distribution pattern can be identified, reflecting the heterogeneous topography of the AP. The maximum elevation of the catchments and the FA factors are also listed in Table S1 in the Supplement.

### 4.4 Cluster analysis

The resulting dendrogram of the hierarchical cluster analysis is plotted in Fig. 6. Four groups are distinguished. The box plots of each input variable are generated based on this grouping and are shown in Fig. 7. The characteristics of the groups are discussed in Sect. 5.3.

## 5 Discussion

Most of the observed glaciers (62 %) retreated and only 8 % advanced in the study period. These findings are comparable to the results of Cook et al. (2005, 2014, 2016). Only glaciers along the west coast showed stable or advancing calving fronts and all glaciers on the east coast receded since 1985. This heterogeneous area change pattern was also observed by Davies et al. (2012) on western Trinity Peninsula. Most significant retreat occurred in sector East-Ice-Shelf. In the period 1985–1995, the Larsen Inlet tributaries (APPE glaciers) lost  $45.0 \text{ km}^2$  of ice. After the disintegration of Prince Gustav and Larsen A Ice Shelf, the tributaries rapidly retreated in the period 1995–2005. The recession slowed down in the latest observation interval (2005–2010). This trend is comparable to detailed observations by Seehaus et al. (2015, 2016) at individual glaciers (DBE glaciers and Sjøgren Inlet glaciers). In sector East the highest area-loss is found in the earliest observation interval (1985–1990). Davies et al. (2012) also reported higher retreat rates for most of the glaciers in this sector in the period 1988–2001 than in the period 2001–2009. However, another significant recession is also found in sector East after 1995 (Fig. 4). Davies et al. (2012) and Hulbe et al. (2004) supposed that the disintegration of a nearby ice shelf affects the local climate. The air temperatures would rise due to the presence of more ice-free water in summers. Thus, the higher retreat rates in sector East after 1995 could be indirectly caused by the disintegration of Prince Gustav and Larsen A Ice Shelf in Sector East-Ice-Shelf. At Base Marambio,  $\sim 100 \text{ km}$  east of this sector, approximately  $2^\circ\text{C}$  higher mean annual air temperatures were recorded in the period 1996–2005 as compared to the period 1986–1995 (Oliva et al., 2017). Unfortunately, no tempera-

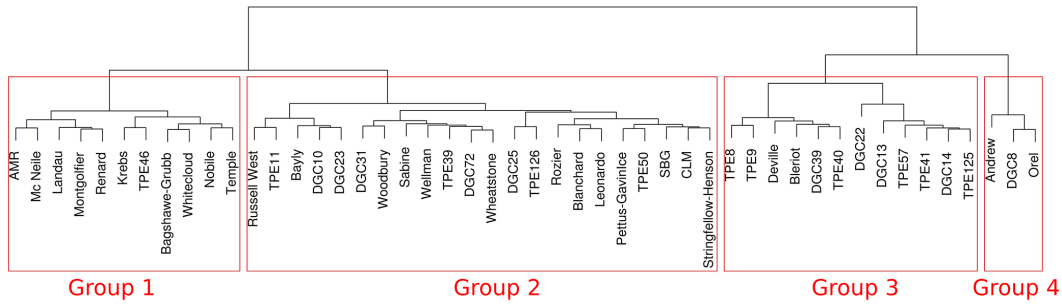


**Figure 6.** Dendrogram of hierarchical cluster analysis of glaciers in sector West. The glaciers are assorted in four groups (red rectangles). See also Sect. 5.3.

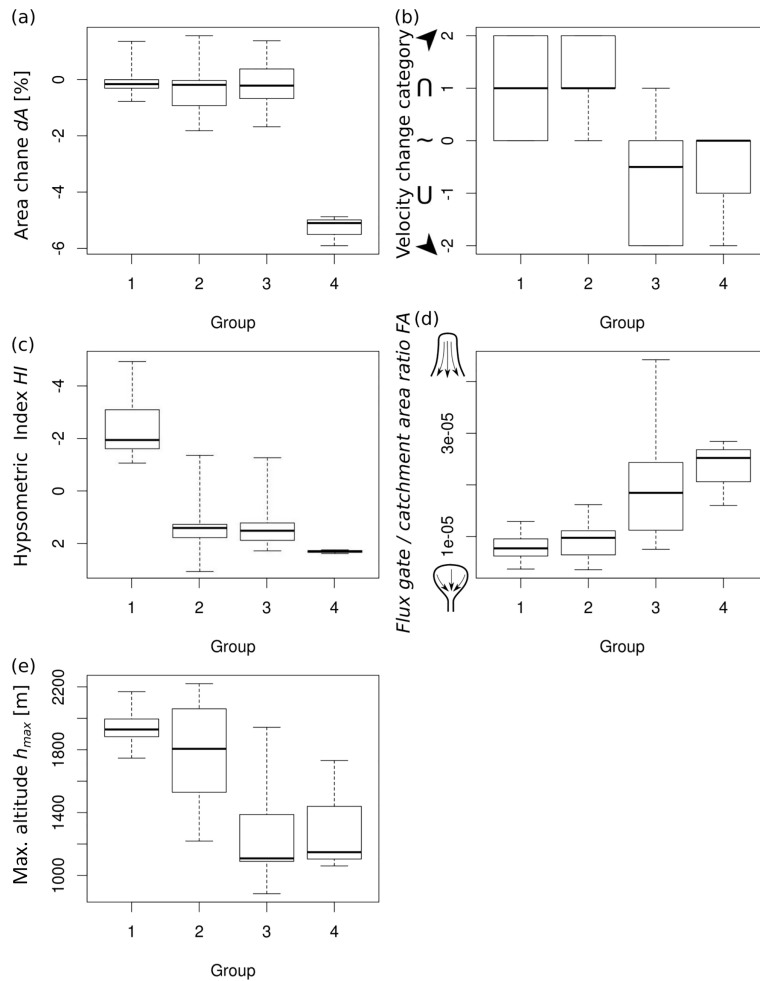


**Figure 7.** Box plots of cluster analysis input variables (sector West) for each group. Whiskers extend to the most extreme data points. (b) The symbols used for the velocity change categories (see Table 3) are the same as in Fig. 3. (d) The pictograms illustrate the catchment shape (see Sect. 3.3).

ture data recorded within sector East are available covering this period that could be used to validate this hypothesis.

The average changes of flow velocities at each sector also vary strongly (Table 5) in the observation period 1992–2014. On the west coast an increase of 41 % is found, whereas in

sector East the glaciers slowed down by approximately 58 % and at the ice shelf tributaries the ice flow increased on average by 26 %. Pritchard and Vaughan (2007) reported an increase in mean flow rate of 7.8 % in frame 4923 (the central and much of the northern part of sector West) and 15.2 % in

frame 4941 (the southern part of sector West) for the period 1992–2005 (frame numbers correspond to European Space Agency convention for identifying ERS coverage). This spatial trend corresponds to our observations, since most of the glaciers which accelerated are located at the southern end of sector West. However, for the same observation period we derived a mean increase in flow velocity by 18.9% in sector West, which is an approximately 1.6 times higher acceleration. Pritchard and Vaughan (2007) estimated the mean velocity change by measuring the flow speed at profiles along the flow direction of the glacier, whereas we measured the velocity across glacier profiles at the terminus. If a tidewater glacier speeds up due to the destabilization of its front, the highest acceleration is found at the terminus (see Seehaus et al., 2015, Fig. 3). Consequently, the different profile locations explain the deviations between both studies.

In the following section the observed changes in the individual sectors are discussed in more detail.

### 5.1 East

The glaciers north of the former Prince Gustav Ice Shelf show a general deceleration. Eyrie, Russell East, TPE130, TPE31, TPE32, TPE34 and 2731 glaciers experienced a rapid decrease and, except 2731 Glacier, a subsequent stabilization or even gentle acceleration of flow velocities (Figs. S2, S6, S7 and S9–S12 in the Supplement). A significant retreat followed by a stabilization or slight re-advance of the calving front position is also observed at these glaciers. According to Benn and Evans (1998), a small retreat of a glacier with an overdeepening behind its grounding line (i.e., where the bed slopes away from the ice front) can result in a rapid recession into the deepening fjord. The increased calving and retreat of the ice front cause stronger up-glacier driving stress, higher flow speed as well as glacier thinning and steepening (Meier and Post, 1987; Veen, 2002). The glacier front stabilizes when the grounding line reaches shallower bathymetry and ice flow also starts to slowdown. A delay between the front stabilization and slowdown can be caused by thinning and steepening of the glacier. Additionally, the accelerated ice flow can surpass the retreat rates and cause short-term glacier advances in the period of high flow speeds (e.g., Eyrie, Russell East, TPE130 and TPE32 glaciers; Figs. S6, S7, S9 and S11 in the Supplement) (Meier and Post, 1987). This process can be initiated by climatic forcing (Benn and Evans, 1998). Significant higher surface air temperature at the northeastern AP and a cooling trend in the 21st century was reported by Oliva et al. (2017) and Turner et al. (2016) (see Sect. 1). Hence, we assume that the initial recessions of the glaciers in sector East were forced by the warming observed by Oliva et al. (2017) and Skvarca et al. (1998) since the 1970s. Therefore, this initial frontal destabilization and retreat led to high flow speeds at the beginning of our ice dynamics time series (earliest velocity measurements from 1992) and the subsequently ob-

served frontal stabilization (after 1985) caused the deceleration of the ice flow. The fjord geometry significantly affects the dynamics of the terminus of a tidewater glacier (Benn and Evans, 1998; Van der Veen, 2002). The tongues of Aitkenhead and 2707 glaciers are split into two branches by nunataks, resulting in rather complex fjord geometries. A retreat from pinning points (e.g., fjord narrowing) causes further rapid recession and higher flow speeds until the ice front reaches a new stable position as observed at 2707 and Aitkenhead Glacier (Figs. S1 and S3 in the Supplement). At TPE10 Glacier (Figs. S8 and S82 in the Supplement) a “peaked” flow velocity evolution is observed as at Aitkenhead Glacier (Figs. S3 and S77 in the Supplement). No nunatak is present at the terminus, but small rock outcrops, indicating a shallow bedrock bump, are identified north of the center of the ice front by visual inspection of optical satellite imagery. Most probably, this shallow bedrock acts as a pinning point and prevents further retreat. The front of Broad Valley Glacier (Fig. S4 in the Supplement) is located in a widening fjord. This geometry makes the glacier less vulnerable to frontal changes (Benn and Evans, 1998). Therefore, no significant changes in flow velocities are observed as a consequence of the frontal recession and re-advance.

Diplock and Victory glaciers (Figs. S5 and S13 in the Supplement) show a decrease of flow speed during retreat (1995–2010) followed by an acceleration combined with frontal advance (2010–2015). Surge-type glaciers (tidewater as well as land terminating) found in various regions worldwide show similar behavior (Meier and Post, 1969; Sevestre and Benn, 2015). They are characterized by episodically rapid down-wasting, resulting in a frontal acceleration and strong advance. Regarding tidewater glaciers the advance can be strongly compensated by increased calving rates in deepwater in front of the glacier. It is therefore possible that these glaciers may have experienced a surge cycle in our observation period; however, a longer time series analysis is necessary to prove this hypothesis.

### 5.2 East-Ice-Shelf

In sector East-Ice-Shelf the tributary glaciers in the Larsen A embayment (2558, Arron Icefall, DBE, Drygalski, LAB2, LAB32, TPE61 and TPE62; Figs. S14, S17, S19–S22, S25 and S26 in the Supplement) and Sjögren Inlet (Boydell, Sjögren and TPE114; Figs. S18, S23 and S24 in the Supplement) lost the downstream Larsen A and Prince Gustav ice shelves in 1995. Nearly all glaciers showed a rapid and significant acceleration after ice shelf breakup and a subsequent slowdown. A gentle peak in flow speeds is obtained at LAB32 and TPE114 glaciers. They are classified as stable because the variations are below the threshold of  $0.25 \text{ m d}^{-1}$ , according to the categorization in Table 3. Dramatic speed-up with subsequent deceleration of former ice shelf tributaries was reported by various authors: e.g., in this sector by Seehaus et al. (2015, 2016) at DBE and Sjögren Inlet

glaciers and further south at Larsen B embayment by Rott et al. (2011) and Wuite et al. (2015). The velocities reported by Rott et al. (2014) at Sjögren, Pyke, Edgeworth and Drygalski glaciers are generally higher than our findings. The authors measured the velocities at locations near the center of the glacier fronts, where the ice flow velocities are typically highest, whereas we measured the median velocities at cross profiles close to the glacier fronts (Seehaus et al., 2015). The different approaches result in different absolute values (see also Sect. S1 in the Supplement), but comparable temporal developments in glacier flow speeds are observed by both author groups. For example, Rott et al. (2015) presented surface velocity measured along a central flow line of Drygalski Glacier. Figure S149 shows our surface velocity measurements across the terminus of Drygalski Glacier and Fig. S94 in the Supplement velocity measurements at the maximum ice thickness across the terminus profile. Both studies show comparable values (e.g., in 1995: this study  $\sim 2.7 \text{ m d}^{-1}$ , Rott et al. (2015)  $\sim 2.8 \text{ m d}^{-1}$ ; in 2009: this study  $\sim 5.5 \text{ m d}^{-1}$ , Rott et al. (2015)  $\sim 6.0 \text{ m d}^{-1}$ ) at the terminus.

Highest peak values of  $6.3 \text{ m d}^{-1}$  are found at TPE61 Glacier in November 1995 and January 1996. Most glaciers (Arron Icefall, Drygalski, LAB2, TPE61, TPE62) strongly decelerated after the initial acceleration and show almost constant flow speeds in recent years, indicating that the glaciers adjusted to the new boundary conditions, albeit significant higher flow speeds (compared to pre-ice-shelf-collapse conditions) can be observed at the central sections of the terminus (see Sect. S1 and Fig. S149 in the Supplement). At 2558, Boydell, DBE and Sjögren glaciers the deceleration is ongoing and Boydell and DBE glaciers still show increased flow speeds at the glacier fronts. We suppose that these tributary glaciers show a prolonged response to ice shelf disintegration, caused by local settings (e.g., bedrock topography or fjord geometry), and are still adjusting to the new boundary conditions, as suggested by Seehaus et al. (2015, 2016).

In the 1980s, Prince Gustav Ice Shelf gradually retreated (see Fig. 1) and 2668 Glacier (Fig. S15 in the Supplement) has not been buttressed by the ice shelf since the early 1990s. A deceleration is found in the period 2005–2010. Hence, this glacier may also have experienced a speed-up in the early 1990s due to the recession of Prince Gustav Ice Shelf in the 1980s. However, the earliest velocity measurement at 2668 Glacier is only available from February 1996.

The ice shelf in Larsen Inlet disintegrated in 1987–1988 and earliest velocity measurements are obtained in 1993. As for 2668 Glacier no sufficient cloud-free coverage by Landsat imagery is available which facilitates the computation of surface velocities for the 1980s. The ice flow speeds at APPE glaciers (Fig. S16 in the Supplement) are nearly stable with short-term variations in the order of  $0.2\text{--}0.5 \text{ m d}^{-1}$  between 1993 and 2014. Rott et al. (2014) also found nearly constant flow velocities at Pyke Glacier (part of the APPE basin, Table 1). The authors suggest that the ice flow of APPE glaciers was not strongly disturbed by the ice shelf removal due to the

steep glacier surfaces and shallow seabed topography at the glacier fronts (Pudsey et al., 2001).

### 5.3 West

The glacier geometries differ strongly along the west coast. In the southern part of sector West the shoreline is more ragged and islands are near the coast. An impact of the islands on the climatic conditions at the AP mainland's coastline (e.g., orographic barrier) is not obvious (visual inspection of RACMO2.3 5.5 km grid cell model results; Van Wessem et al., 2016). However, the climatic conditions on the AP show strong spatial and temporal variability (see Sects. 1 and 3.3). These factors cause the heterogeneous spatial pattern of area and flow speed changes in sector West as compared to the eastern sectors.

Kunz et al. (2012) observed thinning at the glacier termini along the western AP, by analyzing airborne and spaceborne stereo imagery in the period 1947–2010. Two of the 12 studied glaciers are located within our study area: Leonardo Glacier (1968–2010) and Rozier Glacier (1968–2010). An acceleration and terminus retreat can be caused by frontal thinning as shown by Benn et al. (2007). However, Benn et al. (2007) also point out that changes in ice thickness do not necessarily affect the ice flow and that calving front positions and ice dynamics are strongly dependent on the fjord and glacier geometries, derived from modeling results which have higher uncertainties especially for smaller basins.

The large number of glaciers in this sector is analyzed by means of a hierarchical cluster analysis (Sect. 3.4) and assorted into four groups based on the resulting dendrogram (Fig. 6). Box plots of the individual input variables of each group are shown in Fig. 7. The correlation between the observed ice dynamics and the glacier geometries of each group are discussed in the following sections (see also Fig. 7).

#### 5.3.1 Group 1 (14 glaciers)

Most glaciers experienced acceleration in the period 1992–2014. The majority of the glacier basins are “very top heavy” or “top heavy” (median HI =  $-1.8$ ), stretching from sea level up to 1892 m on average. The  $b_{\text{clim}}$  increases toward higher altitudes (Van Wessem et al., 2016) and highest values are found in the zone between 1000 and 1700 m a.s.l. Consequently these glaciers receive high mass input in their large high altitude accumulation areas. The accumulation is known to have significantly increased on the AP by 20 % since 1850 (Thomas et al., 2008). Pritchard and Vaughan (2007) reported that only a small fraction of the acceleration can be attributed to glacier thickening due to increased mass input. Up-glacier thickening combined with frontal thinning (reported by Kunz et al., 2012) leads to a steepening of the glacier and an increase in driving stress, resulting in faster ice flow (Meier and Post, 1987) as observed in this study. Moreover, a thinning of the terminus reduces the effective

basal stress of a tidewater glacier and facilitates faster ice flow (Pritchard and Vaughan, 2007). The flux gate cross sections to catchment size ratios are relatively small, indicating narrowing catchments towards the ice front. The channelized increased ice flow almost compensates for the increased calving rates (due to frontal thinning), resulting in an average recession of the glaciers by only 0.2 % in the period 1985–2015. The high flow speeds may outweigh the calving and lead to ice-front advances as measured at Krebs and TPE46 glaciers. The glacier termini of this group are typically located in narrow fjords (Fig. 5) and are clustered in Charcot, Charlotte and Andvord bays.

### 5.3.2 Group 2 (19 glaciers)

Glaciers of group 2 are spread all over sector West, with a local clustering in Wilhelmina Bay. Group 2 shows similar  $h_{\max}$  and FA characteristics to group 1. Area changes are also quite small (−0.1 %). Most of the glaciers experienced acceleration or show a “peaked” evolution of the flow velocities. In contrast to group 1 the catchments are in general “bottom heavy” and some are even “very bottom heavy”. We assume that the constraints are similar to group 1 (increasing  $b_{\text{clim}}$ , frontal thinning and steepening). However, the additional mass accumulation in the upper areas is smaller due to the bottom-heavy glacier geometries. Consequently, the imbalance due to the frontal thinning and up-glacier mass gain is less pronounced as in group 1 and numerous glaciers (“peak” type) started to decelerate after the speed-up, indicating that these glaciers are adjusting to the new boundary conditions.

### 5.3.3 Group 3 (13 glaciers)

These basins typically show a bottom-heavy hypsometry and smaller elevation ranges (on average up to 1103 m a.s.l.). Thus,  $b_{\text{clim}}$  is relatively low. The smaller mean ice thickness at the termini (161 m, compared to 211 m of all glaciers) of group 3 implies less interaction with the ocean, leading to a small average frontal retreat of  $\sim 0.1$  %. The low frontal ablation does not significantly affect the ice flow, probably due to the flat glacier topography and the low mass input. Consequently, the flow speed is in general stable or even slightly decreases in the observation period. Glaciers of group 3 usually face the open ocean and do not terminate in narrow fjords (especially in the northern part, Trinity Peninsula).

### 5.3.4 Group 4 (3 glaciers)

All basins in this group have a very bottom-heavy hypsometry and an elevation range comparable to group 3 glaciers. The FA factors are in general higher than in group 3, implying that outflow of the catchments is less channelized and the glacier fronts are long compared to the catchment sizes. Therefore, the largest relative area changes, on average −5.1 %, are found at glaciers in group 4. However, the

absolute frontal retreat is small and does not significantly affect the glacier flow. Note that group 4 consists of only three samples, limiting the significance.

## 6 Conclusions

Our analysis expands on previous work (Pritchard and Vaughan, 2007) on ice dynamic changes along the west coast of AP between TPE8 and Bagshawe–Grubb glaciers, in regard to both temporal coverage and analysis methods. It also spatially extends previous work on changes in ice dynamics along the east coast between Eyrie Bay and the Seal Nunataks. The spatially and temporally detailed analysis of changes in ice flow speeds (1992–2014) and ice-front positions (1985–2015) reveals varying temporal evolution in glacier dynamics along the northern AP. The results are in general in line with findings of the previous studies; however, along the west coast a more accelerated glacier flow is determined and on the eastern side temporal evolution of ice dynamics of 21 glaciers is observed for the first time. A large variety of temporal variations in glacier dynamics were observed in our studied area and attributed to different forcing and boundary conditions.

On the east side all glacier fronts retreated in the study period (relative to 1985, relative to 1995 for former Larsen A and Prince Gustav ice shelf tributaries; see also Sect. 5.2), with highest retreat rates observed at former tributaries of the Prince Gustav, Larsen Inlet and Larsen A ice shelves. Moreover, nearly all the glaciers affected by ice shelf disintegration showed similar temporal evolutions of ice velocities. The glaciers reacted with a strong acceleration to ice shelf breakup followed by a deceleration, indicating that the glaciers adjusted or are still adjusting to the new boundary conditions. Glaciers on the east coast north of the former Prince Gustav Ice Shelf showed in general a significant deceleration and a reduction in frontal ablation. Based on the observed warming trend since the 1960s and the subsequent cooling since the mid-2000s in the northern AP, we suggest that the initial recession and speed-up of the glaciers took place before the start of our observation and that the glaciers are now close to a new equilibrium.

The average flow speed of the glaciers along the west coast of the Antarctic Peninsula significantly increased in the observation period but the total frontal change is negligible. No general evolution in ice dynamics of the glaciers at the west coast is obvious. However, correlations between the changes in ice dynamics and the glacier geometries of the individual catchments are obtained by applying a hierarchical cluster analysis. Thus, the geometry of the individual glacier basin strongly affects the reaction of the glacier to external forcing.

We conclude that for regions with such a strong spatial variation in topographic and climatic parameters as the AP, it is impossible to derive a regional trend in glacier change by simply analyzing individual glaciers in this region. There-

fore further detailed observation of the glaciological changes along the AP is needed. Upcoming sensors hopefully facilitate the region-wide measurement of recent surface elevation, since current estimates have got only partial coverage or have got some issues due to the complex topography of the AP. Moreover, future activities should link remote-sensing-derived ice dynamics and glacier extent with ocean parameters and ocean models, as well as regional climate models and ice dynamic models, in order to provide a better quantification of mass changes and physical processes leading to the observed changes.

*Data availability.* Surface velocity fields and terminus profiles are available upon request. Please contact Thorsten Seehaus for this purpose (thorsten.seehaus@fau.de). Various glacier outline data are available at the Antarctic Digital Database (<https://www.add.scar.org/>) and upon request from Alison Cook (alison.cook@durham.ac.uk) and Aline B. Silva (linebsilvaa@gmail.com). The ASTER Global DEM of the Antarctic Peninsula is available at NSIDC doi:10.5060/D47P8W9D. The Antarctic Peninsula bed rock map is available at doi:10.5194/tc-8-1261-2014.

**The Supplement related to this article is available online at <https://doi.org/10.5194/tc-12-577-2018-supplement>.**

*Author contributions.* TS designed the study, processed the SAR data, performed the data analysis and led the writing of the manuscript, in which he received support from all authors. AC and AS compiled and provided glacier front position data sets. MB initiated the project and coordinated the research.

*Competing interests.* The authors declare that they have no conflict of interest.

*Acknowledgements.* This work was supported by the Deutsche Forschungsgemeinschaft (DFG) in the framework of the priority programme “Antarctic Research with comparative investigations in Arctic ice areas” by a grant to Matthias Braun (BR 2105/9-1). Matthias Braun and Thorsten Seehaus would like to thank the HGF Alliance “Remote Sensing of Earth System Dynamics” (HA-310) and Marie-Curie-Network International Research Staff Exchange Scheme IMCONet (EU FP7-PEOPLE-2012-IRSES) for additional support. Access to satellite data was kindly provided by various space agencies, e.g., under ESA AO 4032, DLR TerraSAR-X Background Mission Antarctic Peninsula and Ice Shelves, TSX AO LAN0013, TanDEM-X Mission TDX AO XTI\_GLAC0264, ASF, GLIMS as well as NASA and USGS.

Edited by: Olaf Eisen

Reviewed by: two anonymous referees

## References

- Barrand, N. E., Hindmarsh, R. C. A., Arthern, R. J., Williams, C. R., Mouginit, J., Scheuchl, B., Rignot, E., Ligtenberg, S. R. M., Van Den Broeke, M. R., Edwards, T. L., Cook, A. J., and Simonsen, S. B.: Computing the volume response of the Antarctic Peninsula ice sheet to warming scenarios to 2200, *J. Glaciol.*, 59, 397–409, <https://doi.org/10.3189/2013JoG12J139>, 2013a.
- Barrand, N. E., Vaughan, D. G., Steiner, N., Tedesco, M., Kuipers Munneke, P., van den Broeke, M. R., and Hosking, J. S.: Trends in Antarctic Peninsula surface melting conditions from observations and regional climate modeling, *J. Geophys. Res.-Earth*, 118, 315–330, <https://doi.org/10.1029/2012JF002559>, 2013b.
- Benn, D. I. and Evans, D. J. A.: *Glaciers and Glaciation*, Arnold, London, UK, 734 pp., 1998.
- Benn, D. I., Hulton, N. R. J., and Mottram, R. H.: “Calving laws”, “sliding laws” and the stability of tidewater glaciers, *Ann. Glaciol.*, 46, 123–130, <https://doi.org/10.3189/172756407782871161>, 2007.
- Braun, M. and Humbert, A.: Recent retreat of Wilkins Ice Shelf reveals new insights in ice shelf breakup mechanisms, *IEEE Geosci. Remote S.*, 6, 263–267, <https://doi.org/10.1109/LGRS.2008.2011925>, 2009.
- Berthier, E., Scambos, T. A., and Shuman, C. A.: Mass loss of Larsen B tributary glaciers (Antarctic Peninsula) unabated since 2002, *Geophys. Res. Lett.*, 39, L13501, <https://doi.org/10.1029/2012GL051755>, 2012.
- Burgess, E. W., Forster, R. R., Larsen, C. F., and Braun, M.: Surge dynamics on Bering Glacier, Alaska, in 2008–2011, *The Cryosphere*, 6, 1251–1262, <https://doi.org/10.5194/tc-6-1251-2012>, 2012.
- Cape, M. R., Vernet, M., Skvarca, P., Marinsek, S., Scambos, T., and Domack, E.: Foehn winds link climate-driven warming to ice shelf evolution in Antarctica, *J. Geophys. Res.-Atmos.*, 2015JD023465, <https://doi.org/10.1002/2015JD023465>, 2015.
- Cook, A. J. and Vaughan, D. G.: Overview of areal changes of the ice shelves on the Antarctic Peninsula over the past 50 years, *The Cryosphere*, 4, 77–98, <https://doi.org/10.5194/tc-4-77-2010>, 2010.
- Cook, A. J., Fox, A. J., Vaughan, D. G., and Ferrigno, J. G.: Retreating glacier fronts on the Antarctic Peninsula over the past half-century, *Science*, 308, 541–544, <https://doi.org/10.1126/science.1104235>, 2005.
- Cook, A. J., Murray, T., Luckman, A., Vaughan, D. G., and Barrand, N. E.: A new 100-m Digital Elevation Model of the Antarctic Peninsula derived from ASTER Global DEM: methods and accuracy assessment, *Earth Syst. Sci. Data*, 4, 129–142, <https://doi.org/10.5194/essd-4-129-2012>, 2012.
- Cook, A. J., Vaughan, D. G., Luckman, A. J., and Murray, T.: A new Antarctic Peninsula glacier basin inventory and observed area changes since the 1940s, *Antarct. Sci.*, 26, 614–624, <https://doi.org/10.1017/S0954102014000200>, 2014.
- Cook, A. J., Holland, P. R., Meredith, M. P., Murray, T., Luckman, A., and Vaughan, D. G.: Ocean forcing of glacier retreat in the western Antarctic Peninsula, *Science*, 353, 283–286, <https://doi.org/10.1126/science.aae0017>, 2016.
- Davies, B. J., Carrivick, J. L., Glasser, N. F., Hambrey, M. J., and Smellie, J. L.: Variable glacier response to atmospheric warming, northern Antarctic Peninsula, 1988–2009, *The Cryosphere*, 6, 1031–1048, <https://doi.org/10.5194/tc-6-1031-2012>, 2012.

- De Angelis, H. and Skvarca, P.: Glacier surge after ice shelf collapse, *Science*, 299, 1560–1562, <https://doi.org/10.1126/science.1077987>, 2003.
- de Lange, R., Luckman, A., and Murray, T.: Improvement of satellite radar feature tracking for ice velocity derivation by spatial frequency filtering, *IEEE T. Geosci. Remote*, 45, 2309–2318, <https://doi.org/10.1109/TGRS.2007.896615>, 2007.
- Dee, D. P., Uppala, S. M., Simmons, A. J., Berrisford, P., Poli, P., Kobayashi, S., Andrae, U., Balmaseda, M. A., Balsamo, G., Bauer, P., Bechtold, P., Beljaars, A. C. M., van de Berg, L., Bidlot, J., Bormann, N., Delsol, C., Dragani, R., Fuentes, M., Geer, A. J., Haimberger, L., Healy, S. B., Hersbach, H., Hólm, E. V., Isaksen, I., Kållberg, P., Köhler, M., Matricardi, M., McNally, A. P., Monge-Sanz, B. M., Morcrette, J.-J., Park, B.-K., Peubey, C., de Rosnay, P., Tavolato, C., Thépaut, J.-N., and Vitart, F.: The ERA-Interim reanalysis: configuration and performance of the data assimilation system, *Q. J. Roy. Meteor. Soc.*, 137, 553–597, <https://doi.org/10.1002/qj.828>, 2011.
- Deza, E. and Deza, M. M.: *Encyclopedia of Distances*, Springer, Berlin, Heidelberg, 2009.
- Doake, C. S. M. and Vaughan, D. G.: Rapid disintegration of the Wordie Ice Shelf in response to atmospheric warming, *Nature*, 350, 328–330, <https://doi.org/10.1038/350328a0>, 1991.
- Ferrigno, J. G., Cook, A. J., Foley, K. M., Williams Jr., R. S., Swinbank, Charles, Fox, A. J., Thomson, J. W., and Sievers, J.: Coastal-change and glaciological map of the Trinity Peninsula area and South Shetland Islands, Antarctica-1843-2001: U.S. Geological Survey Geologic Investigations Series Map I-2600-A, 1 map sheet, 32 pp., 2006.
- Fretwell, P., Pritchard, H. D., Vaughan, D. G., Bamber, J. L., Barand, N. E., Bell, R., Bianchi, C., Bingham, R. G., Blankenship, D. D., Casassa, G., Catania, G., Callens, D., Conway, H., Cook, A. J., Corr, H. F. J., Damaske, D., Damm, V., Ferraccioli, F., Forsberg, R., Fujita, S., Gim, Y., Gogineni, P., Griggs, J. A., Hindmarsh, R. C. A., Holmlund, P., Holt, J. W., Jacobel, R. W., Jenkins, A., Jokat, W., Jordan, T., King, E. C., Kohler, J., Krabill, W., Riger-Kusk, M., Langley, K. A., Leitchenkov, G., Leuschen, C., Luyendyk, B. P., Matsuoka, K., Mougint, J., Nitsche, F. O., Nogi, Y., Nost, O. A., Popov, S. V., Rignot, E., Rippin, D. M., Rivera, A., Roberts, J., Ross, N., Siegert, M. J., Smith, A. M., Steinhage, D., Studinger, M., Sun, B., Tinto, B. K., Welch, B. C., Wilson, D., Young, D. A., Xiangbin, C., and Zirizzotti, A.: Bedmap2: improved ice bed, surface and thickness datasets for Antarctica, *The Cryosphere*, 7, 375–393, <https://doi.org/10.5194/tc-7-375-2013>, 2013.
- Goodwin, B. P.: *Recent Environmental Changes on the Antarctic Peninsula as Recorded in an Ice Core from the Bruce Plateau*, The Ohio State University, Columbus, OH, 247 pp., 2013.
- Holland, P. R., Brisbourne, A., Corr, H. F. J., McGrath, D., Purdon, K., Paden, J., Fricker, H. A., Paolo, F. S., and Fleming, A. H.: Oceanic and atmospheric forcing of Larsen C Ice-Shelf thinning, *The Cryosphere*, 9, 1005–1024, <https://doi.org/10.5194/tc-9-1005-2015>, 2015.
- Huber, J., Cook, A. J., Paul, F., and Zemp, M.: A complete glacier inventory of the Antarctic Peninsula based on Landsat 7 images from 2000 to 2002 and other preexisting data sets, *Earth Syst. Sci. Data*, 9, 115–131, <https://doi.org/10.5194/essd-9-115-2017>, 2017.
- Hulbe, C. L., MacAyeal, D. R., Denton, G. H., Kleman, J., and Lowell, T. V.: Catastrophic ice shelf breakup as the source of Heinrich event icebergs, *Paleoceanography*, 19, PA1004, <https://doi.org/10.1029/2003PA000890>, 2004.
- Huss, M. and Farinotti, D.: A high-resolution bedrock map for the Antarctic Peninsula, *The Cryosphere*, 8, 1261–1273, <https://doi.org/10.5194/tc-8-1261-2014>, 2014.
- Jiskoot, H., Curran, C. J., Tessler, D. L., and Shenton, L. R.: Changes in Clemenceau Icefield and Chaba Group glaciers, Canada, related to hypsometry, tributary detachment, length-slope and area-aspect relations, *Ann. Glaciol.*, 50, 133–143, <https://doi.org/10.3189/172756410790595796>, 2009.
- Kaufman, L. and Rousseeuw, P. J.: *Finding groups in data: an introduction to cluster analysis*, Wiley Series in Probability and Mathematical Statistics, Wiley, New York, 1990.
- Kunz, M., King, M. A., Mills, J. P., Miller, P. E., Fox, A. J., Vaughan, D. G., and Marsh, S. H.: Multi-decadal glacier surface lowering in the Antarctic Peninsula, *Geophys. Res. Lett.*, 39, L19502, <https://doi.org/10.1029/2012GL052823>, 2012.
- Lance, G. N. and Williams, W. T.: A general theory of classificatory sorting strategies: II. Clustering systems, *Comput. J.*, 10, 271–277, <https://doi.org/10.1093/comjnl/10.3.271>, 1967.
- Lai, Z. and Huang, M.: Numerical classification of glaciers in China by means of glaciological indices at the equilibrium line, in: *Snow Cover and Glacier Variations*, Proceedings of a Symposium held in Baltimore, Maryland, 10–19 May 1989, IAHS Publication 183, 103–111, 1989.
- Marshall, G. J., Orr, A., van Lipzig, N. P. M., and King, J. C.: The Impact of a changing Southern Hemisphere annular mode on Antarctic Peninsula summer temperatures, *J. Climate*, 19, 5388–5404, <https://doi.org/10.1175/JCLI3844.1>, 2006.
- McNabb, R. W., Hock, R., O’Neel, S., Rasmussen, L. A., Ahn, Y., Braun, M., Conway, H., Herreid, S., Joughin, I., Pfeffer, W. T., Smith, B. E., and Truffer, M.: Using surface velocities to calculate ice thickness and bed topography: a case study at Columbia Glacier, Alaska, USA, *J. Glaciol.*, 58, 1151–1164, <https://doi.org/10.3189/2012JoG11J249>, 2012.
- Meier, M. F. and Post, A.: What are glacier surges?, *Can. J. Earth Sci.*, 6, 807–817, <https://doi.org/10.1139/e69-081>, 1969.
- Meier, M. F. and Post, A.: Fast tidewater glaciers, *J. Geophys. Res.-Sol. Ea.*, 92, 9051–9058, <https://doi.org/10.1029/JB092iB09p09051>, 1987.
- Milligan, G. W. and Cooper, M. C.: A study of standardization of variables in cluster analysis, *J. Classif.*, 5, 181–204, <https://doi.org/10.1007/BF01897163>, 1988.
- Oliva, M., Navarro, F., Hrbáček, F., Hernández, A., Nývlt, D., Pereira, P., Ruiz-Fernández, J., and Trigo, R.: Recent regional climate cooling on the Antarctic Peninsula and associated impacts on the cryosphere, *Sci. Total Environ.*, 580, 210–223, <https://doi.org/10.1016/j.scitotenv.2016.12.030>, 2017.
- Potocki, M., Mayewski, P. A., Kurbatov, A., Handley, M., Simoes, J. C., and Jaña, R.: Detailed glaciochemical records from a northern Antarctic Peninsula site – Detroit Plateau, AGU Fall Meet., San Francisco, 5–9 December 2011, Abstr. 43, 2011.
- Pritchard, H. D. and Vaughan, D. G.: Widespread acceleration of tidewater glaciers on the Antarctic Peninsula, *J. Geophys. Res.*, 112, <https://doi.org/10.1029/2006JF000597>, 2007.
- Pudsey, C. J., Evans, J., Domack, E. W., Morris, P., and Valle, R. A. D.: Bathymetry and acoustic facies be-

- neath the former Larsen-A and Prince Gustav ice shelves, north-west Weddell Sea, *Antarct. Sci.*, 13, 312–322, <https://doi.org/10.1017/S095410200100044X>, 2001.
- Rack, W. and Rott, H.: Further retreat of the Northern Larsen Ice Shelf and collapse of Larsen B, in: 16th International Workshop of the Forum for Research on Ice Shelf Processes (FRISP), Cambridge, 25 June 2003.
- Rack, W. and Rott, H.: Pattern of retreat and disintegration of the Larsen B Ice Shelf, *Antarctic Peninsula*, *Ann. Glaciol.*, 39, 505–510, 2004.
- Rack, W., Rott, H., Nagler, T., and Skvarca, P.: Areal changes and motion of Northern Larsen Ice Shelf, *Antarctic Peninsula*, in: *Geoscience and Remote Sensing Symposium Proceedings Seattle*, 1998, IGARSS'98, IEEE International, 2243–2245, 1998.
- Rau, F. and Braun, M.: The regional distribution of the dry-snow zone on the Antarctic Peninsula north of 70° S, *Ann. Glaciol.*, 34, 95–100, <https://doi.org/10.3189/172756402781817914>, 2002.
- Rignot, E., Casassa, G., Gogineni, P., Krabill, W., Rivera, A., and Thomas, R.: Accelerated ice discharge from the Antarctic Peninsula following the collapse of Larsen B Ice Shelf, *Geophys. Res. Lett.*, 31, <https://doi.org/10.1029/2004GL020697>, 2004.
- Rott, H., Skvarca, P., and Nagler, T.: Rapid collapse of Northern Larsen Ice Shelf, *Antarctica*, *Science*, 271, 788–792, <https://doi.org/10.1126/science.271.5250.788>, 1996.
- Rott, H., Müller, F., Nagler, T., and Floricioiu, D.: The imbalance of glaciers after disintegration of Larsen-B ice shelf, *Antarctic Peninsula*, *The Cryosphere*, 5, 125–134, <https://doi.org/10.5194/tc-5-125-2011>, 2011.
- Rott, H., Floricioiu, D., Wuite, J., Scheiblauer, S., Nagler, T., and Kern, M.: Mass changes of outlet glaciers along the Nordensjököld Coast, northern Antarctic Peninsula, based on TanDEM-X satellite measurements, *Geophys. Res. Lett.*, 2014GL061613, <https://doi.org/10.1002/2014GL061613>, 2014.
- Rott, H., Wuite, J., Floricioiu, D., Nagler, T., and Scheiblauer, S.: Synergy of TanDEM-X DEM differencing and input-output method for glacier monitoring, in: 2015 IEEE International Geoscience and Remote Sensing Symposium (IGARSS), Presented at the 2015 IEEE International Geoscience and Remote Sensing Symposium (IGARSS), Milan, 26–31 July 2015, 5216–5219, <https://doi.org/10.1109/IGARSS.2015.7327010>, 2015.
- Sagredo, E. A. and Lowell, T. V.: Climatology of Andean glaciers: a framework to understand glacier response to climate change, *Global Planet. Change*, 101–109, 2012.
- Scambos, T., Hulbe, C., and Fahnestock, M.: Climate-induced ice shelf disintegration in the Antarctic Peninsula, in: *Antarctic Peninsula Climate Variability: Historical and Paleoenvironmental Perspectives*, edited by: Domack, E., Levente, A., Burnet, A., Bindschadler, R., Convey, P., and Kirby, M., American Geophysical Union, Washington, DC, 79–92, 2003.
- Shepherd, A., Ivins, E. R., A. G., Barletta, V. R., Bentley, M. J., Bettadpur, S., Briggs, K. H., Bromwich, D. H., Forsberg, R., Galin, N., Horwath, M., Jacobs, S., Joughin, I., King, M. A., Lenaerts, J. T. M., Li, J., Ligtenberg, S. R. M., Luckman, A., Luthcke, S. B., McMillan, M., Meister, R., Milne, G., Mouginot, J., Muir, A., Nicolas, J. P., Paden, J., Payne, A. J., Pritchard, H., Rignot, E., Rott, H., Sørensen, L. S., Scambos, T. A., Scheuchl, B., Schrama, E. J. O., Smith, B., Sundal, A. V., Angelen, J. H. van, Berg, W. J. van de, Broeke, M. R. van den, Vaughan, D. G., Velicogna, I., Wahr, J., Whitehouse, P. L., Wingham, D. J., Yi, D., Young, D., and Zwally, H. J.: A Reconciled Estimate of Ice-Sheet Mass Balance, *Science* 338, 1183–1189, <https://doi.org/10.1126/science.1228102>, 2012.
- Scambos, T. A., Berthier, E., Haran, T., Shuman, C. A., Cook, A. J., Ligtenberg, S. R. M., and Bohlander, J.: Detailed ice loss pattern in the northern Antarctic Peninsula: widespread decline driven by ice front retreats, *The Cryosphere*, 8, 2135–2145, <https://doi.org/10.5194/tc-8-2135-2014>, 2014.
- Seehaus, T., Marinsek, S., Helm, V., Skvarca, P., and Braun, M.: Changes in ice dynamics, elevation and mass discharge of Dinsmoor–Bombardier–Edgeworth glacier system, *Antarctic Peninsula*, *Earth Planet. Sc. Lett.*, 427, 125–135, <https://doi.org/10.1016/j.epsl.2015.06.047>, 2015.
- Seehaus, T. C., Marinsek, S., Skvarca, P., van Wessem, J. M., Reijmer, C. H., Seco, J. L., and Braun, M. H.: Dynamic response of Sjøgren Inlet Glaciers, *Antarctic Peninsula*, to ice shelf breakup derived from multi-mission remote sensing time series, *Front. Earth Sci.*, 4, <https://doi.org/10.3389/feart.2016.00066>, 2016.
- Sevestre, H. and Benn, D. I.: Climatic and geometric controls on the global distribution of surge-type glaciers: implications for a unifying model of surging, *J. Glaciol.*, 61, 646–662, <https://doi.org/10.3189/2015JoG14J136>, 2015.
- Skvarca, P., Rott, H., and Nagler, T.: Satellite imagery, a base line for glacier variation study on James Ross Island, *Antarctica*, *Ann. Glaciol.*, 21, 291–296, 1995.
- Skvarca, P., Rack, W., Rott, H., and Ibarzábal y Donángelo, T.: Evidence of recent climatic warming on the eastern Antarctic Peninsula, *Ann. Glaciol.*, 27, 628–632, 1998.
- Skvarca, P., Rack, W., Rott, H., and Donángelo, T. I.: Climatic trend and the retreat and disintegration of ice shelves on the Antarctic Peninsula: an overview, *Polar Res.*, 18, 151–157, 1999.
- Strozzi, T., Luckman, A., Murray, T., Wegmuller, U., and Werner, C. L.: Glacier motion estimation using SAR offset-tracking procedures, *IEEE T. Geosci. Remote*, 40, 2384–2391, <https://doi.org/10.1109/TGRS.2002.805079>, 2002.
- Thomas, E. R., Marshall, G. J., and McConnell, J. R.: A doubling in snow accumulation in the western Antarctic Peninsula since 1850, *Geophys. Res. Lett.*, 35, <https://doi.org/10.1029/2007GL032529>, 2008.
- Turner, J.: Spatial variability of Antarctic Peninsula net surface mass balance, *J. Geophys. Res.*, 107, <https://doi.org/10.1029/2001JD000755>, 2002.
- Turner, J., Colwell, S. R., Marshall, G. J., Lachlan-Cope, T. A., Carleton, A. M., Jones, P. D., Lagun, V., Reid, P. A., and Iagovkina, S.: Antarctic climate change during the last 50 years, *Int. J. Climatol.*, 25, 279–294, <https://doi.org/10.1002/joc.1130>, 2005.
- Turner, J., Lu, H., White, I., King, J. C., Phillips, T., Hosking, J. S., Bracegirdle, T. J., Marshall, G. J., Mulvaney, R., and Deb, P.: Absence of 21st century warming on Antarctic Peninsula consistent with natural variability, *Nature*, 535, 411–415, <https://doi.org/10.1038/nature18645>, 2016.
- van der Veen, C. J.: Calving glaciers, *Prog. Phys. Geog.*, 26, 96–122, <https://doi.org/10.1191/0309133302pp327ra>, 2002.
- van Lipzig, N. P. M., van Meijgaard, E., and Oerlemans, J.: The spatial and temporal variability of the surface mass balance in Antarctica: results from a regional atmospheric climate model, *Int. J. Climatol.*, 22, 1197–1217, <https://doi.org/10.1002/joc.798>, 2002.

- van Lipzig, N. P. M., King, J. C., Lachlan-Cope, T. A., and van den Broeke, M. R.: Precipitation, sublimation, and snow drift in the Antarctic Peninsula region from a regional atmospheric model, *J. Geophys. Res.-Atmos.*, 109, D24106, <https://doi.org/10.1029/2004JD004701>, 2004.
- van Wessem, J. M., Ligtenberg, S. R. M., Reijmer, C. H., van de Berg, W. J., van den Broeke, M. R., Barrand, N. E., Thomas, E. R., Turner, J., Wuite, J., Scambos, T. A., and van Meijgaard, E.: The modelled surface mass balance of the Antarctic Peninsula at 5.5 km horizontal resolution, *The Cryosphere*, 10, 271–285, <https://doi.org/10.5194/tc-10-271-2016>, 2016.
- Ward, J. H.: Hierarchical grouping to optimize an objective function, *J. Am. Stat. Assoc.*, 58, 236–244, <https://doi.org/10.1080/01621459.1963.10500845>, 1963.
- Wendt, J., Rivera, A., Wendt, A., Bown, F., Zamora, R., Casassa, G., and Bravo, C.: Recent ice-surface-elevation changes of Fleming Glacier in response to the removal of the Wordie Ice Shelf, Antarctic Peninsula, *Ann. Glaciol.*, 51, 97–102, 2010.
- Wuite, J., Rott, H., Hetzenecker, M., Floricioiu, D., De Rydt, J., Gudmundsson, G. H., Nagler, T., and Kern, M.: Evolution of surface velocities and ice discharge of Larsen B outlet glaciers from 1995 to 2013, *The Cryosphere*, 9, 957–969, <https://doi.org/10.5194/tc-9-957-2015>, 2015.